Five young star clusters in the outer region of the Small Magellanic Cloud

Andrés E. Piatti,[1]⋆ Ata Sarajedini,[2]⋆ Doug Geisler,[3]⋆ Carme Gallart[4]⋆
and Marina Wischnjewsky†

[1]*Instituto de Astronomía y Física del Espacio, CC 67, Suc. 28, 1428, Ciudad de Buenos Aires, Argentina*
[2]*Department of Astronomy, University of Florida, PO Box 112055, Gainesville, FL 32611, USA*
[3]*Grupo de Astronomía, Departamento de Física, Universidad de Concepción, Casilla 160-C, Concepción, Chile*
[4] *Instituto de Astrofísica de Canarias, Calle Vía Laćtea, E-38200, La Laguna, Tenerife, Spain*

ABSTRACT

Colour–magnitude diagrams in the Washington system are presented for the first time for five star clusters projected on to the outer region of the Small Magellanic Cloud (SMC). The clusters are found to have ages in the range 0.1–1.0 Gyr, as derived from the fit of isochrones with $Z = 0.004$. This sample increases substantially the number of young clusters in the outer SMC – particularly in the south-east quadrant – with well-derived parameters. We combine our results with those for other clusters in the literature to derive as large and homogeneous a data base as possible (totalling 49 clusters) in order to study global effects. We find no conclusive evidence for a dispersion in the cluster ages and metallicities as a function of their distance from the galaxy centre, in the SMC outer region. L 114 and 115, although very distant, are very young clusters, lying in the bridge of the SMC and therefore most likely formed during the interaction which formed this feature. We also find very good agreement between the cluster age–metallicity relation (AMR) and the prediction from a bursting model from Pagel & Tautvaišienė with a burst that occurred 3 Gyr ago. Comparing the present cluster AMR with that derived by Harris & Zaritsky for field stars in the main body of the SMC, we find that field stars and clusters underwent similar chemical enrichment histories during approximately the last couple of Gyr, but their chemical evolution was clearly different between 4 and 10 Gyr ago.

Key words: techniques: photometric – galaxies: individual: Small Magellanic Cloud – Magellanic Clouds – galaxies: star clusters.

1 INTRODUCTION

The Small Magellanic Cloud (SMC) is home to an estimated 2000 star clusters (Hodge 1986). Chiosi et al. (2006) have derived ages with isochrone fitting for the largest sample of clusters (311) in the central part of the galaxy. Other recent studies have considered smaller samples of clusters with some overlap between them: Rafelski & Zaritsky (2005) presented ages for 195 star clusters based on a comparison of integrated colours with simple stellar models; Pessev et al. (2006) have constructed a new data base of near-infrared *JHKs* magnitudes for 75 star clusters; Piatti et al. (2007b) analysed a sample of 44 star clusters composed predominantly of objects with data acquired by our group. As is clear from these results, although cluster ages and metallicities can be derived in a relatively straight-

forward fashion from colour–magnitude diagrams (CMDs), there is still a great deal of work to be done before a complete picture of the formation and evolution history of the SMC cluster system emerges. Several important studies employing the powerful Ca triplet technique to derive metallicities are underway. Initial results from one of these are reported in Kayser et al. (2006) and our group is involved in a similar study (e.g. Geisler et al. 2007). The substantial activity in this field in recent years attests to its astrophysical significance.

Several authors have addressed different issues concerning the SMC star formation history, its chemical enrichment and structural parameters as derived from studies of its star clusters during the last decade. Da Costa & Hatzidimitriou (1998) obtained spectra for seven SMC clusters to determine accurate metal abundances, velocities and their velocity dispersion to study the age–metallicity relation (AMR) and cluster dynamics; Mighell, Sarajedini & French (1998) analysed archival *Hubble Space Telescope* (*HST*) observations of five old star clusters to investigate the age sequence in order to improve our understanding of the formation chronology of the SMC; Rich et al. (2000) reported ages for seven objects from *HST*

⋆E-mail: andres@iafe.uba.ar (AEP); ata@astro.ufl.edu (AS); dgeisler@astro-udec.cl (DG); carme@iac.es (CG)
†Deceased.

images which, joined with previously published data, hinted at the existence of two groups of nearly coeval star clusters and Crowl et al. (2001), using the ages, metal abundances and positions of 12 clusters as proxies, determined the line-of-sight depth of the SMC.

Over the last few years, our group has been conducting a survey of SMC clusters with the aim of enlarging the sample of well-studied objects with ages and metallicities placed on a homogenous scale (Piatti et al. 2001, 2005a,b, 2007a,b,). This program and its continual progression have helped us to improve our understanding of the SMC chemical evolution. As the project was yielding its first results (Piatti et al. 2001), it became clear that the SMC was not formed in a perfect closed box and that there are hints for at least two cluster formation epochs, one at ∼3 and the other at ∼6 Gyr, qualitatively in line with the finding of Rich et al. (2000). Evidence for a bursting formation history for the star clusters was repeatedly confirmed in our subsequent work, and, in particular, Piatti et al. (2005a, 2007b) showed the existence of two main episodes. The most recent burst appears to be concomitant with a close encounter between both Magellanic Clouds (MCs) and the Milky Way (Bekki et al. 2004) ∼3 Gyr ago with the AMRs of both MCs displaying remarkable complementarity (Piatti et al. 2002), since the SMC was actively star forming during the Large Magellanic Cloud (LMC) quiescent age gap epoch. Moreover, we showed (Piatti et al. 2005a) that the SMC remained largely inhomogeneous – chemically speaking – from its birth until approximately 1 Gr ago across its main body. Such inhomogeneity seems to be in agreement with a further result (Piatti et al. 2005b) that the present age–position relation for the SMC clusters in the inner body suggests not only the possibility that the clusters were formed in an 'outside-in' scenario, like a relatively rapid collapse, but also that the inner body itself could have been formed during a bursting formation. The combination of an older and more metal-poor population of clusters distributed throughout the SMC and a younger and metal-richer one mainly formed in the inner body – also shown in Piatti et al. (2007a) – suggests the presence of a radial metal abundance and age gradient for the SMC, with some dispersion. This trend is more notable for the cluster ages than for their metallicities (Piatti et al. 2007a,b).

Here, we present results on five little-studied clusters (Lindsay 106, 108, 111, 114 and 115) located in the outer south-eastern SMC (see Fig. 1), with the aim of adding them to our growing sample of well-studied clusters. Two of them, L 114 and 115, appear to be associated with the SMC bridge. Ahumada et al. (2002) obtained integrated spectra for L 111, 114 and 115, and derived ages of 1 and 5.6 Gyr and 6 Myr, respectively. Matteucci et al. (2002) used CCD BV photometry of stars in the field of L 111 and estimated an age of 600–700 Myr. These are the only previous studies of our sample. Note that three of our targets – L 106, 108 and 111 – are also part of our Ca triplet study, whose results will be presented elsewhere. The next section describes the observations and data reduction. Section 3 presents the procedure followed to estimate the cluster structural parameters, while Section 4 focuses on their CMDs along with the estimation of the cluster properties. The analysis is continued in Section 5 together with a discussion of the results and their implications, which are summarized in Section 6.

2 OBSERVATIONS AND REDUCTIONS

The observational setup and the stellar photometry procedure are identical to that used in Piatti et al. (2007a). To summarize, the CCD images were obtained using the 1.54-m Danish telescope at
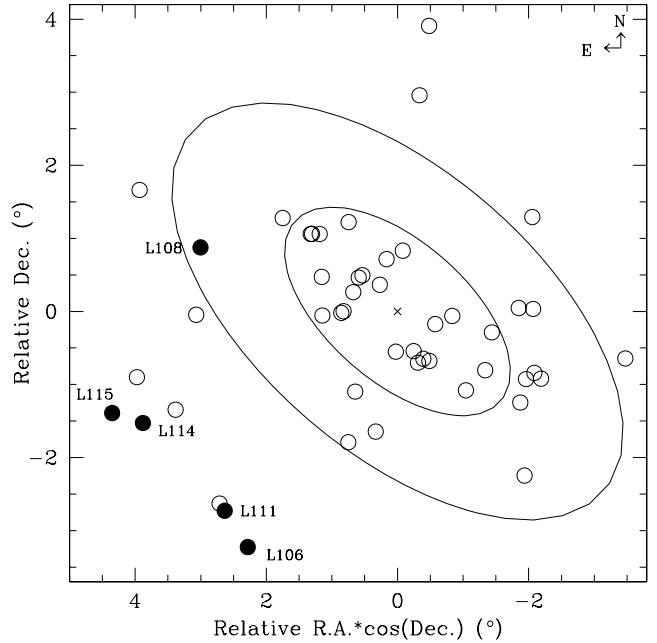
Figure 1. The position of the studied SMC clusters (filled circles) in relation to the SMC optical centre (cross). The semimajor axes of the ellipses drawn in the figure have radii of 2° and 4°, respectively. 44 clusters included in Piatti et al. (2007b) are also shown as open circles.

the European Southern Observatory (ESO) on La Silla, equipped with the Danish Faint Object Spectrograph and Camera (DFOSC). Observations were secured in the Washington C and Kron–Cousins R filters (Canterna 1976). The latter has a significantly higher throughput as compared with the Washington T_1 filter and can be precisely transformed to yield T_1 magnitudes (Geisler 1996). The DFOSC imager has a field-of-view of 13.7×13.7 arcmin^2 with a plate scale of 0.42 arcsec pixel^{-1}. Table 1 shows the log of the observations with filters, exposure times, airmasses and seeing estimates. All of the data were taken under photometric conditions. Standard stars from the list of Geisler (1996) were observed in order to secure the transformation from the instrumental to the standard system. The instrumental signatures (e.g. the bias level and pixel-to-pixel sensitivity variations) in the CCD images were removed using standard observational techniques and tasks in IRAF.

The stellar photometry was performed using the star finding and point spread function (PSF) fitting routines in the DAOPHOT/ALLSTAR suite of programs (Stetson 1987). Radially varying aperture corrections were applied to take out the effects of PSF variations across the field of view, although a quadratically varying PSF was employed. The resultant instrumental magnitudes were standardized using equations similar to those employed by Piatti et al. (1999). The root mean square (rms) deviations of the fitted values from the fits to the standards were all less than 0.015 mag. Fig. 2 shows finding charts of the clusters based on the photometry and Tables 2–6 present the photometry (a sample of Table 2 is given here; the full versions of that tables, and of Tables 3–6, are available online as Supplementary Material).

3 CLUSTER STRUCTURAL PARAMETERS

With the aim of disentangling cluster features from those belonging to their surrounding fields, we started by determining the location of the cluster centres in order to construct stellar density profiles to aid

Table 1. Observation log of selected clusters.

Star cluster[a]	α_{2000} (h m s)	δ_{2000} (° ′ ″)	l (°)	b (°)	Date	Filter	Exposure (s)	Airmass	Seeing (arcsec)
L 106, ESO 29-SC44	1 30 38	−76 03 16	299.82	−40.84	1999 Dec 29	C	1800	1.35	1.6
						R	600	1.31	1.3
L 108	1 31 32	−71 57 10	298.57	−44.83	1999 Dec 29	C	1800	1.27	1.4
						R	600	1.23	1.1
NGC 643, L 111, ESO 29-SC50	1 35 00	−75 33 24	299.34	−41.27	1999 Nov 4	C	1800	1.30	1.8
						R	600	1.27	1.2
L 114, ESO 30-SC5	1 50 19	−74 21 22	297.63	−42.16	1999 Nov 5	C	1800	1.30	1.4
						R	600	1.27	1.2
NGC 796, L 115, ESO 30-SC6	1 56 44	−74 13 10	297.01	−42.15	1999 Nov 4	C	1500	1.27	2.2
						R	500	1.25	1.3

[a]Cluster identifications are from Lindsay (1958, L) and Lauberts (1982, ESO).
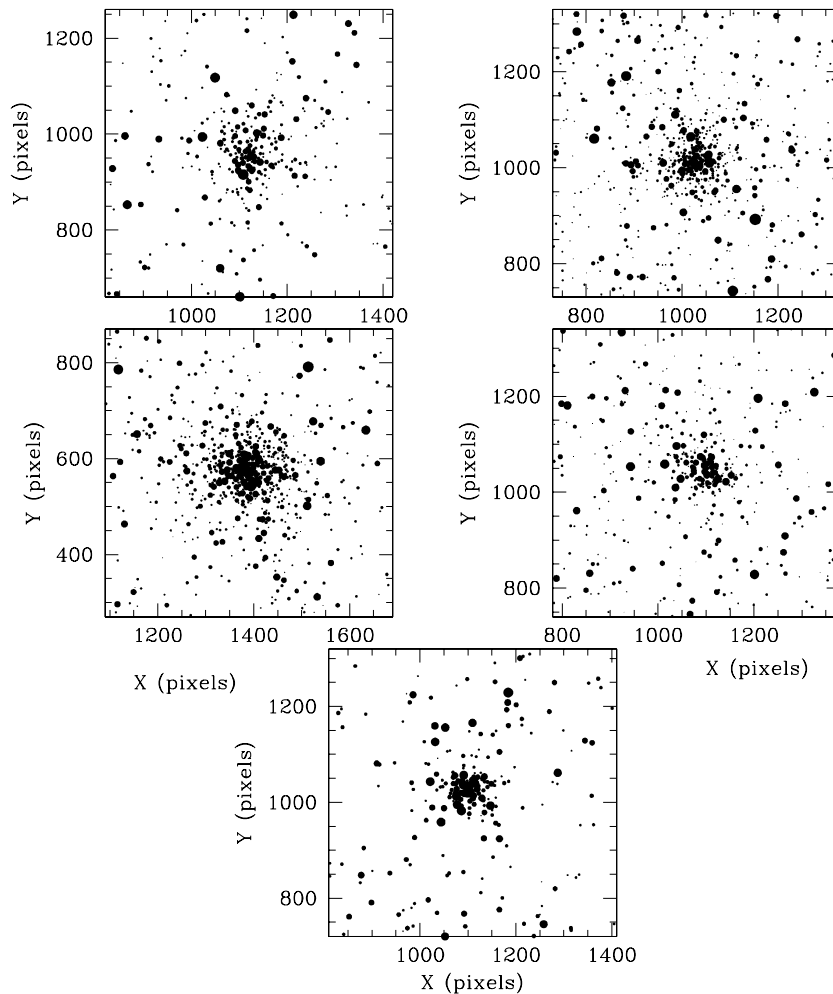
Figure 2. Schematic finding charts for the SMC cluster fields: L 106 (upper left), L 108 (upper right), L 111 (middle left), L 114 (middle right) and L 115 (bottom). North is up and east is to the left. The size of the plotting symbol is proportional to the T_1 brightness of the star.

in the adoption of the optimum cluster radii. This is a straightforward approach which allows us to obtain CMDs dominated by cluster stars but including the unavoidable field contamination. The success of this method depends on the ratio between the number of cluster and field stars at each radius. We have here refined our techniques and used a more quantitative and robust analysis than used in our previous work in this series.

The coordinates of the cluster centres and their estimated uncertainties were determined by fitting Gaussian distributions to the star counts in the *x* and *y* directions for each cluster. The fits of the Gaussians were performed using the NGAUSSFIT routine in the STSDAS/IRAF package, adopting a single Gaussian and fixing the constant to the corresponding background levels (i.e. stellar field densities assumed to be uniform) and the linear terms to zero. The centre

Table 2. A sample table of CCD CT_1 data of stars in the field of L 106. The full version of the table is available as Supplementary Material.

Star	X (pixel)	Y (pixel)	T_1 (mag)	$\sigma(T_1)$ (mag)	$C - T_1$ (mag)	$\sigma(C - T_1)$ (mag)
. . .	. . .	. . .	. . .	. . .	. . .	. . .
11	231.72	26.01	18.614	0.019	1.351	0.022
12	812.10	26.10	19.968	0.015	0.495	0.020
13	663.04	31.22	20.164	0.017	1.329	0.032
14	33.17	32.27	17.020	0.025	1.747	0.029
15	1710.10	32.73	20.433	0.036	1.469	0.054
. . .	. . .	. . .	. . .	. . .	. . .	. . .
. . .	. . .	. . .	. . .	. . .	. . .	. . .
. . .	. . .	. . .	. . .	. . .	. . .	. . .

Note. (X, Y) coordinates correspond to the reference system of Fig. 2. Magnitude and colour errors are the standard deviation of the mean, or else the observed photometric errors for stars with one measurement.

of the Gaussian, its amplitude and its full width at half-maximum (FWHM) acted as variables. The number of stars projected along the *x* and *y* directions was counted in intervals of 50 pixel. In addition, we checked that using smaller (from 25 pixel) and larger (up to 100 pixel) spatial bins does not produce significant changes in the derived centres. We iterated the fitting procedure once on average,

after eliminating a couple of discrepant points. Cluster centres were finally determined with a typical standard deviation of ± 6 pixel (~ 2.5 arcsec) in all cases.

We then constructed the cluster radial profiles based on counts of stars in boxes 50 pixel on a side, distributed throughout the field. The selected box size allowed us to sample the spatial star distribution statistically and avoid spurious effects, mainly caused by the presence of localized groups, rows or columns of stars. Thus, the number of stars per unit area at a given radius *r* can be directly calculated through the expression

$$(n_{r+25} - n_{r-25})/\left[(m_{r+25} - m_{r-25}) \times 50^2\right],$$

where n_j and m_j represent the number of stars and boxes included in a circle of radius *j*, respectively. Note that the method does not necessarily require a complete circle of radius *r* within the observed field to be able to estimate the mean stellar density at that distance. This is an important consideration since having a stellar density profile which reliably extends far away from the cluster allows us to estimate the background level with high precision, which is necessary (i) to derive the cluster radius, defined as the distance from the cluster centre where the stellar density profile intersects the background level; (ii) to measure the FWHM of the stellar density profile, which plays a significant role – from a stellar content point of view – in the construction of the cluster CMDs; (iii) to investigate the possible existence of asymmetries in the density of stars in
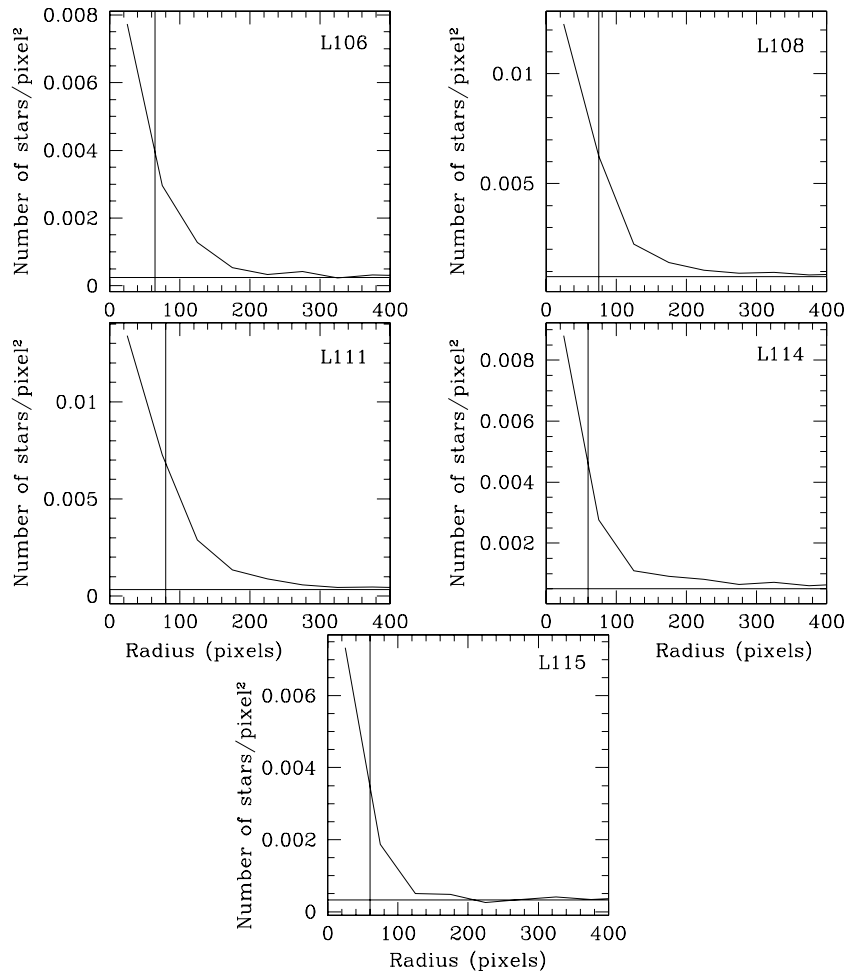
Figure 3. Stellar density profiles for the selected clusters. Panel distribution is as in Fig. 2. The horizontal line corresponds to the background level far from the cluster, whereas the vertical line indicates r_{FWHM}.
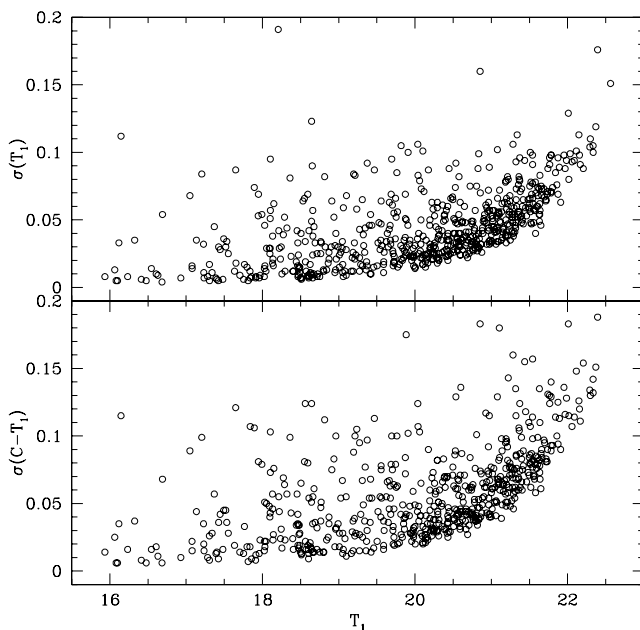
Table 7. Cluster sizes and field contamination.

Name	Background ($\times 10^5$) (star pixel^{-2})	r_{FWHM} (pixel)	r_{cls} (pixel)	Field contamination (per cent)		
				$r < r_{FWHM}$	$r_{FWHM} < r < 200$ pixel	200 pixel $< r < r_{cls}$
L 106	24 ± 5	65	450	4	26	78
L 108	77 ± 8	75	600	8	42	83
L 111	33 ± 5	80	600	3	16	64
L 114	51 ± 7	60	550	9	51	76
L 115	33 ± 4	60	200	7	67	100

the outskirts of clusters and (iv) to estimate the percentage of field contamination.

The resulting density profiles expressed as number of stars per unit area in pixels are shown in Fig. 3. Here, we have illustrated the region around the centre of each cluster so that the profiles extend out to only 400 pixel. Table 7 lists the calculated background levels, the radii at the FWHM, the cluster radii and the field contamination estimated in percentage for different radial intervals. The background regions were delimited by an inner circle of radius 600 pixel from the cluster centres and the observed field boundaries. All of the background levels are significantly lower than the central cluster densities, as expected since clusters are relatively populous and are placed in the outer region of the SMC. However, the percentage of field stars rapidly increases from the cluster core regions outwards, indicating the relatively small sizes of the clusters. Only L 106 and 111 strongly dominate over their surrounding fields at a radial range from r_{FWHM} to 200 pixel from their centres.

Besides field contamination, the quality of the photometry was also taken into account in order to evaluate the influence of photometric errors on the cluster principal sequences in the CMDs. The T_1 magnitude and $C - T_1$ colour errors provided by DAOPHOT II for all five studied clusters are shown in Fig. 4. We only plot the errors for stars within $r < r_{FWHM}$, where cluster stars prevail. We recall that, due to the crowding in these areas, the photometric errors of these stars are generally larger than those for stars located further away.
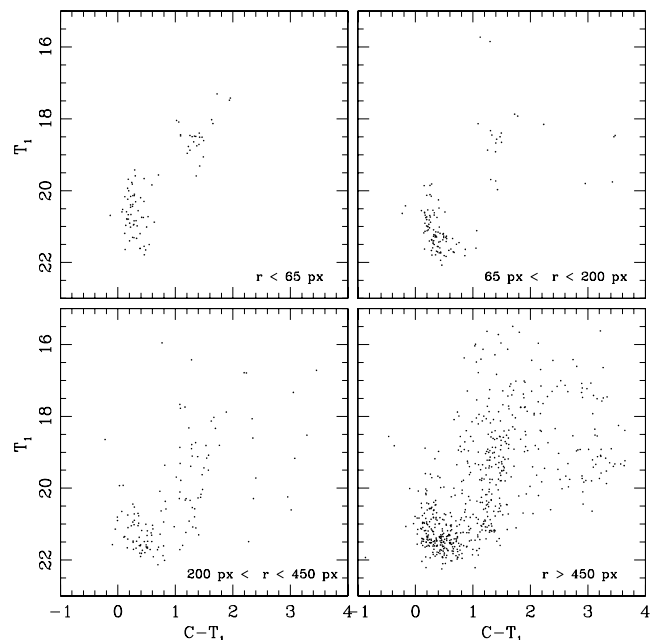
Even so, the mean magnitude and colour errors for stars brighter than $T_1 = 19$ are in the range $\langle \sigma(T_1) \rangle = 0.005$–$0.05$ and $\langle \sigma(C - T_1) \rangle = 0.005$–$0.07$; for stars with $T_1 = 19$–22.5, $\langle \sigma(T_1) \rangle \leqslant 0.13$ and $\langle \sigma(C - T_1) \rangle \leqslant 0.16$. Thus, we assume that using the appropriate radial extractions that isolate as many cluster stars as possible will provide a CMD that is suitable for estimating reliable cluster ages from theoretical isochrone fits.

4 CLUSTER PROPERTIES FROM THE CMDS

We constructed four CMDs covering different circular extractions around each cluster as shown in Figs 5–9. Panels in the figures are arranged in such a way that they document the stellar population variations from the innermost to the outermost regions of the cluster fields from left- to right-hand side and from top to bottom; we start with the CMD for stars distributed within $r < r_{FWHM}$, followed by the cluster regions delimited by $r_{FWHM} < r < 200$ pixel, then the cluster corona (200 pixel $< r < r_{cls}$) and finally the adopted field CMDs ($r > r_{cls}$).

Turning now to a discussion of the cluster CMDs, we begin with the CMD of L 106 in Fig. 5. The surrounding field of L 106 contains populations with a range of ages older than the age of the cluster, as indicated by the well-populated turnoff region from approximately the cluster turnoff magnitude to the magnitude limit of the CMD. The cluster has a subgiant and red giant branch (SG-RGB), and

Figure 4. Magnitude and colour photometric errors as a function of T_1 for $r < r_{FWHM}$ of the associated clusters.

Figure 5. Washington T_1 versus $C - T_1$ CMDs for measured stars in the L 106 cluster field. Extraction radii in pixels are given in each panel.
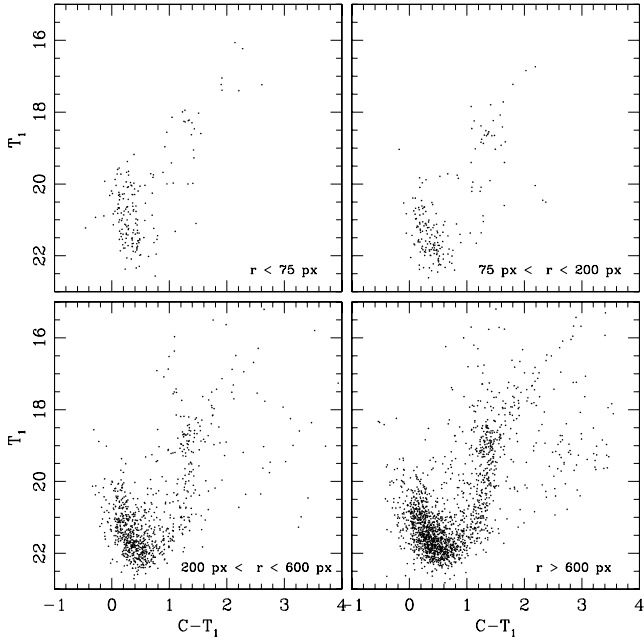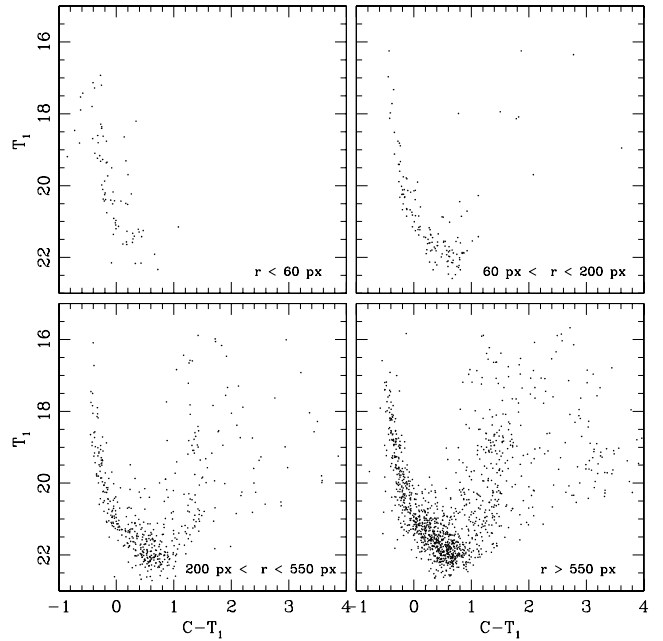
Figure 6. Washington T_1 versus $C - T_1$ CMDs for measured stars in the L 108 cluster field. Extraction radii in pixels are given in each panel.
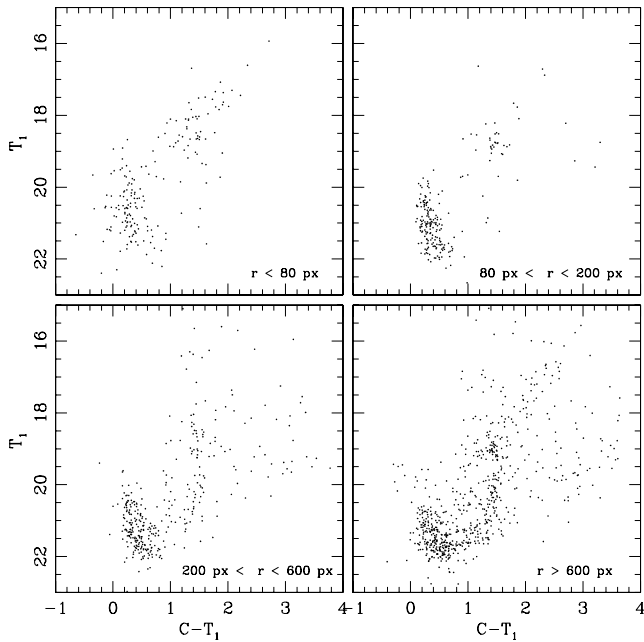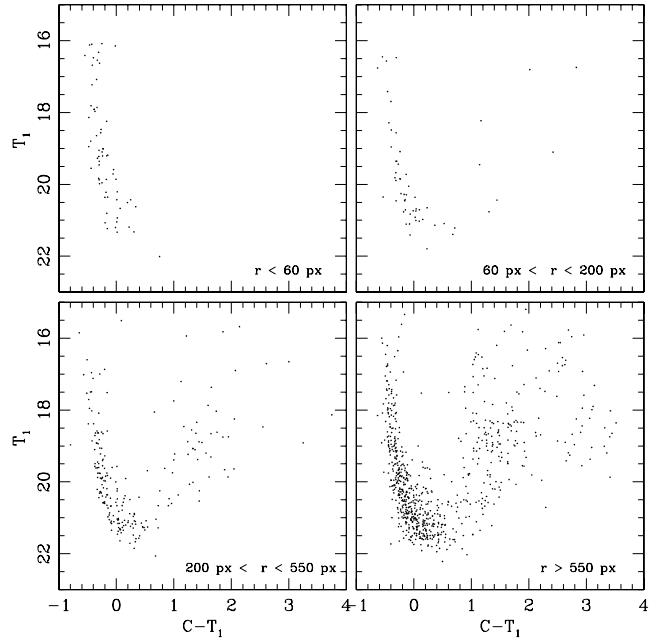

Figure 7. Washington T_1 versus $C - T_1$ CMDs for measured stars in the L 111 cluster field. Extraction radii in pixels are given in each panel.

Figure 8. Washington T_1 versus $C - T_1$ CMDs for measured stars in the L 114 cluster field. Extraction radii in pixels are given in each panel.

Figure 9. Washington T_1 versus $C - T_1$ CMDs for measured stars in the L 115 cluster field. Extraction radii in pixels are given in each panel.

a populous red giant clump (RGC). The cases of L 108 (Fig. 6) and L 111 (Fig. 7) are somewhat similar to L 106; the most notable difference being that the latter clusters have more developed SGBs and RGBs.

In all three cases, it appears that the field population in each large-radius CMD contains a component that is much older than the clusters, but each also contains a component that appears to be roughly coeval with the cluster (or perhaps slightly older). The fields surrounding L 106 and 111 are separated from L 108 by more than

$4°$ on the sky and all of them seem to show relatively similar field CMD features.

L 114 (Fig. 8) and 115 (Fig. 9) are also located in the southeast sector of the SMC outer region – strictly speaking, in the SMC bridge region (Harris 2007) – and separated by between $0°.5$ and $\approx 2°$ from L 106, 108 and 111. Both former clusters and their surrounding fields present well-defined and populous young MSs. The extracted $r < r_{\mathrm{FWHM}}$ CMDs show relatively more scatter in the MS than those for the adjacent extraction, probably due to larger photometric errors caused by crowding effects near the cluster centre. The superposition

Table 8. Fundamental parameters of SMC clusters.

Name	$E(B-V)$ (mag)	Age (Myr)	a (°)
L 106	0.05	890^{+230}_{-100}	7.88
L 108	0.04	890^{+370}_{-180}	4.46
L 111	0.07	1000^{+260}_{-210}	7.83
L 114	0.04	140^{+60}_{-40}	8.54
L 115	0.03	110^{+50}_{-20}	9.11

in the field CMDs of an older stellar population begins to be visible in the outer regions of the clusters and beyond. Harris (2007) also found an old stellar population confined to his *mb2* SMC bridge field, where L 114 and 115 are placed.

Because of the significant field contamination in each circular extraction (see Table 7), in the subsequent analysis, we decided to use the CMDs with $r < 200$ pixel for L 106 and 111, and those for $r < r_{FWHM}$ for L 108, 114 and 115.

To estimate the cluster ages, we fitted theoretical isochrones from Girardi et al. (2002) to the cluster CMDs, once the cluster colour excesses $E(C-T_1)$, metallicities [Fe/H] and distance moduli were fixed. As for the cluster distance moduli, we adopt for all the clusters the value of the SMC distance modulus $(m-M)_o = 18.77 \pm 0.06$ obtained by Crowl et al. (2001). They also found that the line-of-sight depth of the galaxy is approximately 6 kpc. Then, bearing in mind that any cluster of the sample could be placed in front or behind the SMC, we conclude that the difference in its apparent distance modulus would be $\Delta(V-M_V) \sim 0.2$ mag, if a value of 60 kpc is adopted for the mean SMC distance. Given that we estimate an uncertainty of 0.2–0.3 mag in adjusting the isochrones to the cluster CMDs in magnitude, our simple assumption of adopting a unique value for the distance modulus for all of the clusters should not affect the error budget in our final results substantially.

Cluster reddening values were estimated by interpolating the extinction maps of Burstein & Heiles (1982, hereafter BH) and Schlegel, Finkbeiner & Davis (1998, hereafter SFD). BH maps were obtained from H I (21 cm) emission data for the southern sky and provide us with foreground $E(B-V)$ colour excesses which depend on the Galactic coordinates. On the other hand, SFD obtained full-sky maps from 100 μm dust emission and found that at high latitudes, the dust map correlates well with maps of H I emission, but deviations are coherent in the sky and are especially conspicuous in regions where the H I emission saturates towards denser clouds. The difference between the two reddening scales is $\Delta E(B-V) = 0.016 \pm 0.009$, the SFD values being larger. Since we estimate an uncertainty of adjusting the isochrones to the cluster CMDs along the $C-T_1$ colour of 0.05 mag, we assume the values of SFD for the cluster reddenings. These values are listed in Table 8. The $A_{T_1}/E(B-V)$ and $E(C-T_1)/E(B-V)$ ratios given by Geisler & Sarajedini (1999) were then used to enter in the CMDs with the corresponding M_{T_1} and $(C-T_1)_0$ values.

Finally, we selected a subset of isochrones computed taking into account overshooting effects and heavy element content of $Z = 0.004$ and 0.008 ([Fe/H] = -0.7 and -0.4 dex, respectively), taken from the most frequently derived metallicity range of SMC clusters younger than ≈ 1 Gyr (Piatti et al. 2007a). Note that these clusters are all too young ($\leqslant 1$ Gyr) to either derive ages from the δT_1 technique (Geisler et al. 1997) or to derive metallicities from the colour of the RGB in our Washington CMDs (Geisler & Sarajedini 1999). We performed independent fits for both selected metallici-

ties and found that for $Z = 0.008$ the fits result with red giant loops ~ 0.3 mag redder, turnoffs ~ 0.5 mag brighter and ages ~ 190 Myr younger. In the case of L 114 and 115, we found the same turnoff shift and an age difference of ≈ 30 Myr; the $Z = 0.008$ ages being younger. Therefore, we adopt a heavy element content of $Z = 0.004$ for the clusters, and associate to this metallicity an estimated error of ~ 0.2 dex. Fig. 10 shows the results of the isochrone fits, which consisted of successive different isochrone adjustments to the cluster CMDs until finding the one which best resembles the cluster features. The solid lines in Fig. 10 correspond to the isochrones with the adopted clusters ages, whereas the dashed lines are the isochrones which represent the errors in these age estimates. These errors were derived taking into account the observed dispersion in the cluster principal sequences in the CMD (see Table 8). We call attention to the presence of stars brighter than $T_1 \sim 18.5$ mag and with $C - T_1$ from ~ 0.8 to 2 mag spread over the L 111 RGB, which are not predicted by the isochrones.

5 ANALYSIS AND DISCUSSION

Three clusters of the sample (L 111, 114 and 115) were the subject of an integrated spectral analysis by Ahumada et al. (2002). They compared the integrated cluster spectra with template spectra and measured the equivalent widths (EWs) of Balmer lines to obtain the cluster ages. For L 111, they quoted an age of 1.0 ± 0.2 Gyr, while for L 114 and 115 they derived ages of 5.6 ± 0.5 Gyr and 6 ± 10 Myr, respectively. Our present results for L 111 compare well with that of Ahumada et al. – note that Matteucci et al. (2002) also found an age of 600–700 Myr – but are quite different in the cases of L 114 and 115. Figs 8 and 9 show that, while both the cluster and surrounding field CMDs exhibit similar features, the clusters are relatively younger. Therefore, we see two possible reasons for the differences between our age results and those of Ahumada et al. (2002): (i) the possible influence of a very bright star or stars which could bias the cluster integrated spectrum (note that the field contaminations for these two clusters are the largest in our sample) and (ii) the bimodal behaviour of the Balmer line EWs, which reaches a maximum value for $t \sim 400$ Myr and decreases symmetrically towards younger and older ages (Bica & Alloin 1986). Consequently, a very young cluster and a somewhat older cluster could have similar average EWs.

The five studied clusters are located in the outer region of the SMC, considered as the portion of the galaxy more distant than $3°.5$ from its centre (see e.g. Bica & Dutra 2000; Piatti et al. 2005b). On the other hand, viewing the SMC as a triaxial galaxy with the declination, right ascension and line-of-sight as the three axes, Crowl et al. (2001) found axial ratios of approximately 1:2:4. Based on this result, and with the purpose of describing the spatial distribution of the clusters, we decided to use an elliptical framework instead of a spherical one in order to reflect more meaningfully the flattening of the galaxy. Then, here, a is the semimajor axis – parallel to the SMC main body – of an ellipse centred at RA = $00^h 52^m 45^s$, Dec. = $-72°49'43''$ (J2000) (Crowl et al. 2001) and with a b/a ratio of 1/2. Thus, we assume that cluster age or metallicity gradients, if any, correlate much better with a pseudo-elliptical (projected) distance measured from the galaxy centre than with the radial distance, or distances defined along the right ascension or declination axes. For the subsequent analysis, we adopt the semimajor axis a as the representative spatial variable to trace the behaviour of the cluster ages and metallicities throughout the galaxy. The values of a corresponding to the clusters in the present work are between $4°.5$ and $9°.3$ with an average of $7°.6$ (see last column of Table 8). Up until now,
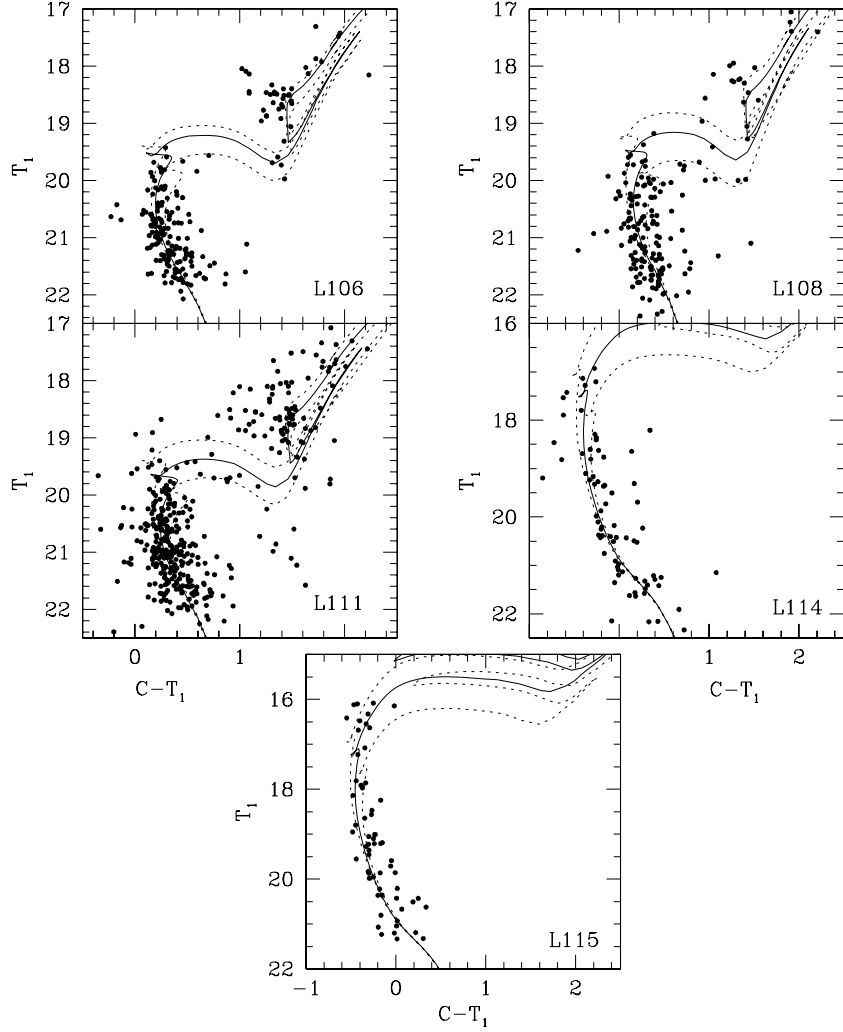
Figure 10. Washington T_1 versus $C - T_1$ CMDs for star clusters. Isochrones from Girardi et al. (2002), computed taking into account overshooting and $Z =$ 0.004, are overplotted. The solid and dashed lines correspond to the derived clusters ages and to the ages obtained taken into account their associated errors (see Column 3 of Table 8), respectively: log $(t) = 8.90$, 8.95 and 9.05 for L 106; 8.85, 8.95 and 9.10 for L 108; 8.90, 9.00 and 9.10 for L 111; 8.00, 8.15 and 8.30 for L 114; 7.95, 8.05 and 8.20 for L 115.

the SMC cluster in our Washington sample (Piatti et al. 2007b) with the largest a value has been L 113 at 7°.8. However, our new clusters L 106, 111, 114 and 115 turn out to be the clusters with the largest a values with ages and metallicities on the same homogeneous scale as the 44 cluster sample of Piatti et al. (2007b). Note that L 114 and 115 are close to the Magellanic bridge region, whose formation is studied in detail by Harris (2007). By adding the present clusters to the sample of Piatti et al., we can now enlarge our study of the chemical evolution of the SMC clusters to cover a wider baseline in semimajor axis and therefore have greater sensitivity to any radial trends. We note here that the present sample is unique in that we only derive ages and not metallicities as well from our photometry, counting on the isochrones to be good metallicity indicators, as was found in Geisler et al. (2003).

The results of Piatti et al. (2007b) confirmed previous suggestions that the further a cluster is from the centre of the SMC, the older and more metal-poor it tends to be, with some dispersion. They drew this conclusion from the measurement of ages and metallicities of two newly identified old clusters (L 110 and 112, $t \sim 6.5$ Gyr) located in the SMC outer region added to their existing data base of

properties for 42 SMC clusters. If we perform a linear fit to their data, avoiding a few outliers, we find slopes for [Fe/H] and age as a function of the semimajor axis of -0.12 ± 0.02 and 1.20 ± 0.15, respectively. Noel et al. (2007) also examined the star formation history of the galaxy from CMDs of 12 star fields located between $\sim 1°$ and $\sim 4°$ in different parts of the SMC. Particularly, they found that intermediate-age and old star populations are distributed throughout the surveyed regions, while those younger are preferably distributed towards the central regions, supporting our results.

However, the presence of relatively young clusters in the outer region – note that the present clusters are the most distant ones yet studied – could provide a new constraint to our understanding of cluster formation in the SMC and galaxy evolution in general. What is more, old clusters could have been formed in the outer region and as a result of their subsequent motions now be actually seen in the inner region (e.g., L 8, NGC 339, 361, 416). Thus, we could partially explain the scatter observed in the age versus semimajor axis plane for old and inner SMC clusters (see e.g. fig. 3 of Piatti et al.), given an initial perfect age gradient. Conversely, young clusters formed in the inner region have not had enough time to move outwards and reach
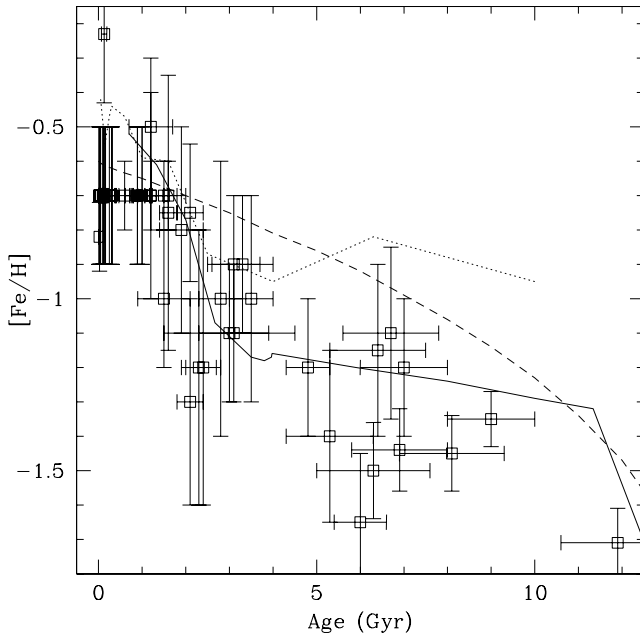
Figure 11. AMR for L 106, 108, 111, 114 and 115 (filled boxes) and the 44 cluster sample of Piatti et al. (2007b) (open boxes). The data are compared with the closed box continuous star formation model (dashed line) computed by Da Costa & Hatzidimitriou (1998), and the bursting model (solid line) of Pagel & Tautvaišienė (1998). The AMR obtained by Harris & Zaritsky (2004) is depicted with a dotted line (see Section 5 for details).

the outer disc, or vice versa; so that we practically see them near their birthplaces. Since we observed young clusters in a particular south-eastern region of the outer SMC, we conclude that relatively recent cluster formation events must have taken place there. A similar result can be drawn for cluster metallicities: chemically enriched gas clouds would also appear to exist in the outermost portion of the galaxy.

These last results could lead us to suppose that apparently neither the age nor the metallicity of clusters in the outer SMC disc is well described in terms of distance from the galaxy centre. However, if we consider the distribution of a total of 49 clusters [44 taken from Piatti et al. (2007b) and the present sample of five studied ones] in the [[Fe/H],a] and [t, a] planes, we find that 15 clusters should be spread outside 1σ from the linear fits found above. Indeed, we counted 16 and 17 clusters in the [[Fe/H],a] and [t, a] planes placed outside 1σ from the fits, respectively. Therefore, although we should not discard the possibility that in the outer body ($a > 3\overset{\circ}{.}5$) metallicity and age gradients could be somewhat negligible or non-existent, we also note that better cluster statistics are needed to draw more conclusive statements.

The present enlarged cluster sample taken together appears to strengthen the observed AMR making it more consistent – within the estimated cluster metallicity errors – with the bursting star formation history of Pagel & Tautvaišienė (1998) rather than to a simple closed system with continuous star formation under the assumption of chemical homogeneity (Da Costa & Hatzidimitriou 1998), although our present sample of five clusters does not add much weight to this result and, in fact taken by themselves, are more consistent with the Da Costa & Hatzidimitriou model. Previous studies favouring the bursting star formation scenario are those of Mighell et al. (1998), Rich et al. (2000), Bekki et al. (2004) and Piatti et al. (2005a), among others. Fig. 11 shows the presently studied clusters

(filled boxes) and the 44 clusters from Piatti et al. (2007b) (open boxes) in the age–metallicity plane, wherein we have superimposed with solid and dashed lines the corresponding models of Pagel & Tautvaišienė and Da Costa & Hatzidimitriou, respectively. We have also added the AMR obtained by Harris & Zaritsky (2004) (dotted line), who spatially resolved the central $4° \times 4\overset{\circ}{.}5$ area of the SMC's main body and studied its star formation and chemical enrichment history using *UBVI* photometry from their MCs Photometric Survey (MCPS). They found that the derived AMR is consistent with that for star clusters (see their fig. 12). However, note that when comparing their MCPS AMR with that provided by Pagel & Tautvaišienė (see Fig. 11), there exists a notable offset of Δ[Fe/H] ~ 0.3 dex in the $t \approx 5$–10 Gyr age range; the latter being more metal-rich. Such a difference is even larger if the presently adopted cluster metallicities are used instead of those assumed by Pagel & Tautvaišienė. The deviation toward higher metallicities at old ages may be due to the limited range of metallicities made available to their fitting routine. On the other hand, the MCPS AMR correlates very well with the cluster AMR for $t < 3$ Gyr.

Very recently, Idiart, Maciel & Da Costa (2007) have derived ages and abundances for $\sim$40 planetary nebulae in the SMC. Their AMR lies to even higher metallicities than the Harris & Zaritsky AMR, by $\sim$0.2 dex. In addition, Kayser et al. (2006) derived Ca triplet abundances for seven SMC clusters. Their preliminary AMR shows general agreement with ours for clusters younger than about 5 Gyr but their two older clusters have metallicities lying at the upper end or above the values we derive for similarly aged clusters. Thirdly, Noel et al. (2007) determined the AMR for a field $1\overset{\circ}{.}1$ to the southeast of the SMC centre using *BR* photometry and a detailed analysis including isochrones and the star formation history. Their AMR is in quite good agreement with ours, over the full age range. Furthermore, their AMR is corroborated by an independent study of the same field using the Ca triplet technique (Carrera 2007).

Thus, these various studies indicate that there still appears to be substantial uncertainty in the derivation of either ages and/or abundances as well as possible zero-point offsets between the different techniques used for different objects. Nonetheless, we can tentatively conclude that SMC field stars and clusters started to undergo similar chemical enrichment histories approximately in the last couple of Gyr, but their chemical evolution was clearly different between 4 and 10 Gyr ago.

6 SUMMARY AND CONCLUSIONS

We have used the 1.54 m Danish telescope at the ESO on La Silla to obtain CCD imaging of a number of star clusters in the SMC as part of a continuing project. Here, we have presented the CMDs of L 106, 108, 111, 114 and 115 in the Washington photometric system. The CMDs are used to estimate ages for the clusters from a comparison to theoretical isochrones. These objects increase substantially the sample of clusters in the outer SMC – particularly in the south-east quadrant – with well-derived parameters, and also extends our sample to larger galactocentric radii.

Combining these results with those from our previous papers, we draw the following conclusions.

(i) There is a dispersion in the cluster ages and metallicities as a function of their distances from the galaxy centre, especially in the SMC outer body. Although old and metal-poor clusters are preferently found in this portion of the galaxy, there are also clusters formed relatively recently with a metal content similar to the present-day value for the inner SMC.

(ii) Independent from the spatial distribution of cluster ages and metallicities and the incompleteness in the cluster sample studied in detail, particularly of clusters younger than 1 Gyr, the bursting star formation paradigm – with a burst which occurred at $t \sim 3$ Gyr – still appears to be the most appropriate to describe the cluster AMR, although there are some differences between different cluster AMR studies.

(iii) Comparing the present cluster AMR with that derived by Harris & Zaritsky (2004) for the main body of the SMC, we find that field stars and clusters started to undergo similar chemical enrichment histories approximately in the last couple of Gyr, but were clearly different between 4 and 10 Gyr ago. These results clearly need to be followed-up with more observations to confirm their robustness.

REFERENCES

Abraham R. G., 1999, in Barnes J. E., Sanders D. B., eds, Proc. IAU Symp. 186, Galaxy Interactions at Low and High Redshift. Kluwer, Dordrecht, p. 11
Ahumada A. V., Clariá J. J., Bica E., Dutra C. M., 2002, A&A, 393, 855
Bekki K., Couch W. J., Beasley M. A., Forbes D.A., Chiba M., Da Costa G. S., 2004, ApJ, 610, L93
Bica E., Alloin D., 1986, A&A, 162, 21
Bica E., Dutra C. M., 2000, AJ, 119, 1214
Burstein D., Heiles C., 1982, AJ, 87, 1165 (BH)
Canterna R., 1976, AJ, 81, 228
Carrera R., 2007, PhD thesis, IAC, Spain
Chiosi E., Vallenari A., Held E. V., Rizzi L., Moretti A., 2006, A&A, 452, 179
Crowl H. H., Sarajedini A., Piatti A. E., Geisler D., Bica E., Clariá J. J., Santos J. F. C., Jr, 2001, AJ, 122, 220
Da Costa G. S., Armandroff T. E., 1990, AJ, 100, 162
Da Costa G. S., Hatzidimitriou D., 1998, AJ, 115, 1934
Geisler D., 1996, AJ, 111, 480
Geisler D., Sarajedini A., 1999, AJ, 117, 308
Geisler D., Bica E., Dottori H., Clariá J. J., Piatti A. E., Santos J. F. C., Jr, 1997, AJ, 114, 1920
Geisler D., Piatti A. E., Bica E., Clariá J. J., 2003, MNRAS, 341, 771
Geisler D., Grocholski A., Sarajedini A., Cole A., Smith V., 2007, in Richtler T., Larsen S., eds, ESO Astrophys. Symp., Globular Clusters-Guides to Galaxies. In press
Girardi L., Bertelli G., Bressan A., Chiosi C., Groenewegen M. A. T., Marigo P., Salasnich B., Weiss A., 2002, A&A, 391, 195
Harris J., 2007, ApJ, 658, 345
Harris J., Zaritsky D., 2004, AJ, 127, 1531
Hodge P. W., 1986, PASP, 98, 1113
Idiart T. P., Maciel W. J., Da Costa R. D., 2007, A&A, 472, 101
Kayser A., Grebel E. K., Harbeck D. R., Cole A. A., Koch A., Gallagher J. S., Da Costa G. S., 2006, preprint (astro-ph/0607047)
Lauberts A., 1982, ESO/Uppsala Survey of the ESO (B) Atlas. European Southern Observatory, Garching bei Munchen
Lindsay E. M., 1958, MNRAS, 118, 172
Matteucci A., Ripepi V., Brocato E., Castellani V., 2002, A&A, 387, 861
Mighell K. J., Sarajedini A., French R. S., 1998, AJ, 116, 2395
Noel N. E. D., Gallart C., Costa E., Mendez R. A., 2007, AJ, 133, 2037
Pagel B. E. J., Tautvaišienė G., 1998, MNRAS, 299, 535
Pessev P. M., Goudfrooij P., Puzia Th. H., Chandar R., 2006, AJ, 132, 781
Piatti A. E., Geisler D., Bica E., Clariá J. J., Santos J. F. C., Jr, Sarajedini A., Dottori H., 1999, AJ, 118, 2865
Piatti A. E., Santos J. F. C. Jr, Clariá J. J., Bica E., Sarajedini A., Geisler D., 2001, MNRAS, 325, 792
Piatti A. E., Sarajedini A., Geisler D., Bica E., Clariá J. J., 2002, MNRAS, 329, 556
Piatti A. E., Sarajedini A., Geisler D., Seguel J., Clark D., 2005a, MNRAS, 358, 1215
Piatti A. E., Santos J. F. C. Jr, Clariá J. J., Bica E., Ahumada A. V., Parisi M. C., 2005b, A&A, 440, 111
Piatti A. E., Sarajedini A., Geisler D., Clark D., Seguel J., 2007a, MNRAS, 377, 300
Piatti A. E., Sarajedini A., Geisler D., Gallart D., Wischnjewsky M., 2007b, MNRAS, 381, L84
Rafelski M., Zaritsky D., 2005, AJ, 129, 2701
Rich R. M., Shara M., Fall M., Zurek D., 2000, AJ, 119, 197
Schlegel D. J., Finkbeiner D. P., Davis M., 1998, ApJ, 500, 525 (SFD)
Stetson P. B., 1987, PASP, 99, 191

SUPPLEMENTARY MATERIAL

The following supplementary material is available for this article:

Table 2. CCD CT_1 data of stars in the field of L 106.
Table 3. CCD T_1 data of stars in the field of L 108.
Table 4. CCD T_1 data of stars in the field of L 111.
Table 5. CCD T_1 data of stars in the field of L 114.
Table 6. CCD T_1 data of stars in the field of L 115.

This material is available as part of the online article from: http://www.blackwell-synergy.com/doi/abs/10.1111/j.1365-2966.2007.12439.x (this link will take you to the article abstract).

Please note: Blackwell Publishing are not responsible for the content or functionality of any supplementary materials supplied by the authors. Any queries (other than missing material) should be directed to the corresponding author for the article.

This paper has been typeset from a TEX/LATEX file prepared by the author.